Dynamic response of post-tensioned rocking structures with inerters

R. Thiers-Moggia[a], C. Málaga-Chuquitaype[a]

[a]*Department of Civil and Environmental Engineering, Imperial College London, UK*

Abstract

Post-tensioned rocking systems have proved to be highly effective in controlling structural damage during strong ground motions. However, recent events have highlighted the importance of looking at both the structural and non-structural components within a holistic framework. In this context, the high rotations and accelerations associated with the rocking motion can cause significant non-structural damage and affect the performance and functionality of the entire system. In this paper, we examine analytically the fundamental dynamics of post-tensioned rocking structures and investigate the benefits of using supplemental rotational inertia to reduce their seismic demands and improve their overall performance. The newly proposed strategy employs inerters, a mechanical device that develops a resisting force proportional to the relative acceleration between its terminals. Analyses conducted for a wide range of acceleration pulses and real pulse-like ground motions show that post-tensioned structures equipped with inerters consistently experience lower demands and have reduced probabilities of exceeding limit states typically associated with damage. Importantly, the new vibration control strategy advanced in this paper opens the door for an expedient modification of the fundamental dynamic response of rocking systems without altering their geometry.

Keywords: Self-centring structures, vibration control, rocking motion, inerter, pulse-like ground motion.

1. Introduction

Controlled rocking of structures can significantly reduce the moments that develop at their base during strong ground shaking. This fact was already recognized by Housner [1], who motivated by the good performance of tall slender structures during several earthquakes, studied the planar dynamic behaviour of rigid bodies and derived analytical equations that describe their rocking motion. During the last decades, this concept has been widely applied to the development of post-tensioned buildings that aim to limit the structural damage during severe earthquakes [2–4]. Popular among these applications are post-tensioned rocking walls [5, 6], where the structural members are free to uplift and rock while post-tensioned tendons are incorporated to increase the lateral strength and recentring capabilities of the structure. Additional energy dissipation can be provided through unbounded mild steel reinforcement or external devices such as U-shaped flexural plates (UFPs) [7].

The structural performance of post-tensioned rocking systems has been extensively studied both analytically and numerically. Pampanin et al. [8] proposed a section analysis method suitable for post-tensioned

Email address: c.malaga@imperial.ac.uk (C. Málaga-Chuquitaype)

connections, while Spieth et al. [9] developed a multi-spring contact element capable of accurately modelling the global behaviour of rocking frames, including local effects such as neutral axis shift. This element was subsequently adapted for the analysis of post-tensioned rocking walls by Pennucci et al. [10]. On the other hand, extensive experimental programmes have been conducted on concrete [7] and timber[11] post-tensioned walls. Their results have shown that post-tensioned systems have good ductility and energy dissipation characteristics, making them an attractive alternative in seismic-prone regions.

Modern design frameworks generally quantify seismic risk in terms of overall performance, looking at both the structural and non-structural components [12]. Although rocking post-tensioned systems have proved to be highly effective in controlling structural damage, very limited attention has been dedicated to the associated rotation and acceleration demands. Vassiliou and Makris[13] built on Housner's model and studied the dynamic response of a vertically restrained solitary rocking column, concluding that post-tensioned tendons can reduce rotation demands in smaller columns subjected to long-period excitations but have little effect on taller structures. However, no assessment of the effects on the acceleration levels was offered. Aragaw and Calvi[14] examined the non-linear response of a set of base-rocking wall buildings and proposed two simplified methodologies to estimate floor acceleration spectra in this type of structures. Their study highlighted the importance of an adequate consideration of seismic accelerations in the design of non-structural elements and points out the necessity for control strategies to limit these demands.

Research on seismic control systems for rocking structures has been mainly oriented to the protection of museum artefacts and non-structural equipment [15–17]. Consequently, most strategies have focused on preventing overturning using simple measures, such as modifying the centre of mass or using fixed and semi-active anchorages [18, 19]. Although these proposals can reduce the overturning vulnerability of free-standing bodies, they can also induce undesirable stresses and are generally not suitable for rocking building structures. Alternative passive approaches have also been proposed by a number of researchers, aiming to reduce the seismic demands without preventing the rocking behaviour. De Leo et al. [20] studied the use of a pendulum mass damper hinged at the top of a rigid block, showing that the system is effective for a limited range of frequencies.

A seismic control strategy that has been gaining increasing attention over the last years is the use of supplemental rotational inertia. Several types of inerters, a mechanical component that develops a resisting force proportional to the relative acceleration between its terminals [21], have been developed and proposed to control vibrations in civil structures[22–27]. Arakaki et al.[28] suggested a damper formed of a cylindrical mass rotating inside a chamber filled with a viscous fluid, while Makris and Kampas [29] and Málaga-Chuquitaype et al. [30] highlighted the benefits of incorporating clutch-inerter systems. All these studies have focused on the protection of fixed-based structures, where the seismic-induced displacements are controlled primarily via stiffness, damping and strength [31, 32]. In the case of rocking structures, the dominant motion is rotational and the seismic stability originates mainly from the difficulty of mobilizing their rotational inertia [33]. In this context, Thiers-Moggia and Málaga-Chuquitaype [34] proposed the use of supplemental rotational inertia to enhance the seismic performance of rocking structures. They showed that the inclusion of inerters effectively reduces the frequency parameter of a block, resulting in lower rotation seismic demands and enhanced stability due to the well-known size effects of the rocking behaviour [1]. However, their study concentrated on the fundamental behaviour of free-rocking structures and did not consider the effects of post-tensioning or the possibility of having different seismic and gravitational masses

as is customary for new building applications.

In this paper we examine the seismic rocking response and associated demands in post-tensioned rigid walls equipped with supplemental rotational inertia devices. Firstly, based on Housner's idealizations we develop a simple single-degree-of-freedom model representative of post-tensioned rocking systems. Secondly, the effect of the vertical tendons in the rocking response of the structure is assessed in terms of maximum rotations and peak angular accelerations for a wide range of pulse excitations. Subsequently, the inerter device is introduced and original equations that describe the rocking motion of the post-tensioned wall-inerter system are derived. In addition to the reductions in rotation and acceleration demands, the effects of the inerter on the base shear are also evaluated. Finally, a probabilistic assessment of the seismic performance of a typical building structure is conducted using a set of 202 pulse-like ground motions obtained from the Pacific Earthquake Engineering Research Center (PEER) database. Our results demonstrate that post-tensioned rocking structures equipped with inerters experience smaller rotation and acceleration demands than unprotected ones and have lower probabilities of exceeding limit states associated with non-structural damage.

2. Fundamental dynamics of a free-standing rocking wall

The free-standing rigid block considered in Housner's [1] early study corresponds to a particular case in which the only mass mobilized by the horizontal and gravity accelerations is the mass of the body itself. This assumption is reasonable for many rocking objects, such as museum artefacts and non structural equipment, but is not usually valid for rocking building structures. In these cases, additional masses attached to the structural elements change the inertial forces and the use of gravity resistance systems (e.g. gravity frames) or in-plane lateral resistance elements (e.g rectangular walls) can modify the ratio between the tributary seismic mass, m_{sis}, and the gravity load, W, exerting the restoring moment (Figure 1).

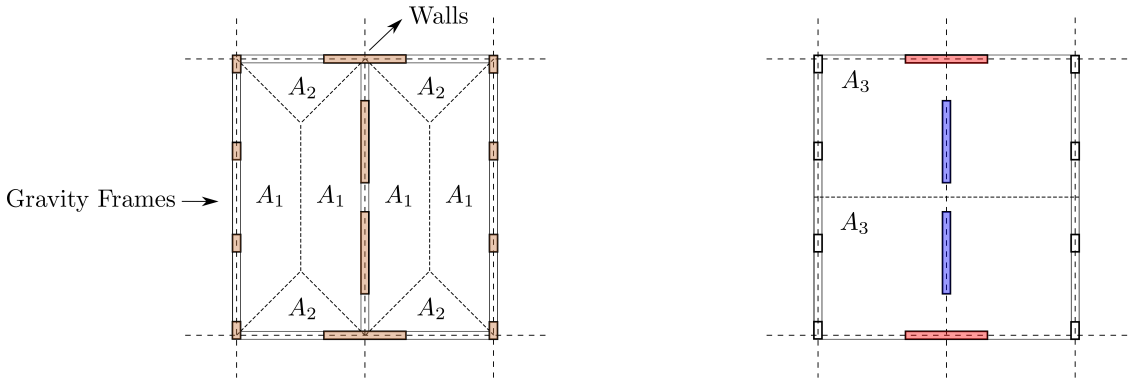

(a) Vertical gravity elements (indicated in brown) and their corresponding tributary areas (A_i).

(b) Seismic mass taken by each lateral resistant element (red: X direction, blue: Y direction).

Figure 1: Example of the distribution of gravity loads and seismic masses in building structures.

The dynamic response of such structures can be better represented by the model depicted in Figure 2, where the rigid free-standing wall is free to rotate about points O and O', and appropriate arrangements to prevent slipping (such as shear keys) have been considered. In addition, the application of rocking systems to building structures generally comprises capacity design procedures for the structural elements. Accordingly,

it is reasonable to assume that the structures will respond in the elastic range. Our study examines the response of such systems considering a simplified model of a rigid body, therefore disregarding the effect of the elastic deformations in the block. It is recognized that these deformations may alter the efficiency of the inerter in very flexible structures, although this problem is beyond the scope of this work If a diaphragm connection with rotational decoupling is assumed (e.g. large diameter pin[35]), the seismic mass and gravity loads can be concentrated and considered to act at point C. The geometry of the wall is characterized by the slenderness α and the size parameter R, while its rotation is measured by the angle θ. Impact is treated following Housner's approach [1], considering the coefficient of restitution as an independent parameter and equal to $\eta = 0.85$. This formulation assumes that impact forces concentrate at the pivot point, dissipating energy instantaneously and causing an immediate change of velocity and infinite acceleration. More recent experimental and analytical studies have shown that the consideration of distributed impact forces lead to a more realistic prediction of the acceleration response[36]. Moreover, it has been shown that in these cases the maximum acceleration demands are governed by the rocking response in between impacts[37]. Consequently, the acceleration spikes predicted by Housner's model are not considered when assessing acceleration demands throughout this paper.

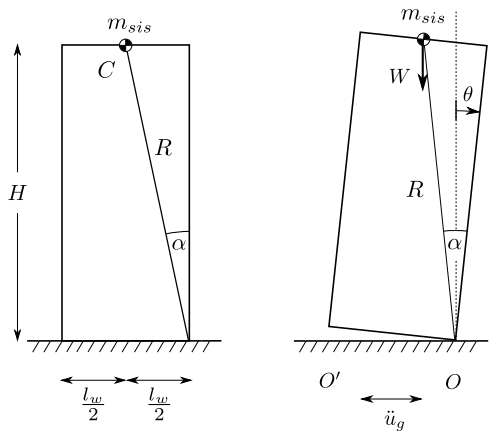

Figure 2: Single-degree-of-freedom system with a concentrated mass on the top and an independent gravity load W, representative of a structural rocking wall.

In most practical building applications the rotational inertia and weight of the rocking element are significantly smaller than the corresponding translational seismic mass, m_{sis}, and tributary gravity load, W, and can be neglected. Then, under a horizontal ground excitation, $\ddot{u}_g$, the rigid wall uplifts and starts rocking if:

$$\ddot{u}_g \geq \frac{g}{m_{ratio}} \tan \alpha \tag{1}$$

where $m_{ratio} = m_{sis}/m_g$ is the ratio between the seismic mass and the gravitational mass associated to the gravity load transferred to the wall (i.e. $m_g = W/g$). Evaluating the rotational equilibrium around the rocking pivot point gives (Figure 2):

$$\ddot{\theta}\, \cancelto{0}{I_0} + m_{sis}\, R^2\, \ddot{\theta} + W R \sin(\alpha\, sgn(\theta) - \theta) = -m_{sis}\, \ddot{u}_g\, R \cos(\alpha\, sgn(\theta) - \theta) \tag{2}$$

The equation above can be rearranged and presented in a compact form:

$$\ddot{\theta} = -p_w^2 \big(\sin(\alpha\, sgn(\theta) - \theta) + m_{ratio}\, \frac{\ddot{u}_g}{g} \cos(\alpha\, sgn(\theta) - \theta) \big) \tag{3}$$

where p_w is the frequency parameter of the rigid rocking element defined as

$$p_w = \sqrt{\frac{g}{R\, m_{ratio}}} \tag{4}$$

2.1. Response scaling and similarity

The dynamic response of the classic rocking block studied by Housner[1] is governed by 4 independent dimensionless parameters[38].

$$\theta_{max} = f\left(\frac{\omega_g}{p}\,,\, \frac{a_g}{g}\,,\, \alpha\,,\, \eta \right) \tag{5}$$

Equation 3 and Equation 4 show that the ratio between the seismic and gravitational masses in a rocking building divide the gravity acceleration, g. Therefore, the response of a rocking building wall is governed by:

$$\theta_{max} = f\left(\frac{\omega_g}{p_w}\,,\, \frac{a_g\, m_{ratio}}{g}\,,\, \alpha\,,\, \eta \right) \tag{6}$$

For most practical applications the wall slenderness, α, will be smaller than 20° (e.g. $l_w = 3[m]$ and $H = 9[m] \rightarrow \alpha = 9.5°$), and the dimension-orientationless properties developed by Dimitrakopoulos and DeJong [38] for slender blocks can be applied:

$$\frac{\theta_{max}\, g}{a_g\, m_{ratio}} = \phi\left(\frac{\omega_g}{p_w}\,,\, \frac{a_g\, m_{ratio}}{g\, \tan\alpha}\,,\, \eta \right) \tag{7}$$

Figure 3 compares the response of two different slender blocks of equivalent dimension-orientationless parameters ($a_g\, m_{ratio}/g \tan\alpha = 23.3$ and $\eta = 0.85$), subjected to a pulse excitation of frequency ratio $\omega_g/p_w = 8$. It is evident from Figure 3 that, when presented in terms of the proposed parameters, the responses collapse into a single master curve.

2.2. Rocking response under pulse excitations

The rocking response of free-standing blocks is usually studied by means of rocking spectra, like the one presented in Figure 4a. This representation consist of contour plots of the normalized response variable in the frequency ratio (ω_g/p_w) and acceleration amplitude plane ($a_g\, m_{ratio}/g \tan\alpha$), for a block of a given slenderness α. In this study, symmetric Ricker wavelets [39, 40] (Equation 8) are used as pulse excitations. This analytical wavelet has been shown to satisfactorily approximate the coherent pulse of several pulse-like ground motions[41].

$$\ddot{u}_g(t) = a_g \left(1 - \frac{2\pi^2 t^2}{T_g^2} \right) e^{-\frac{\pi^2 t^2}{T_g^2}} \tag{8}$$

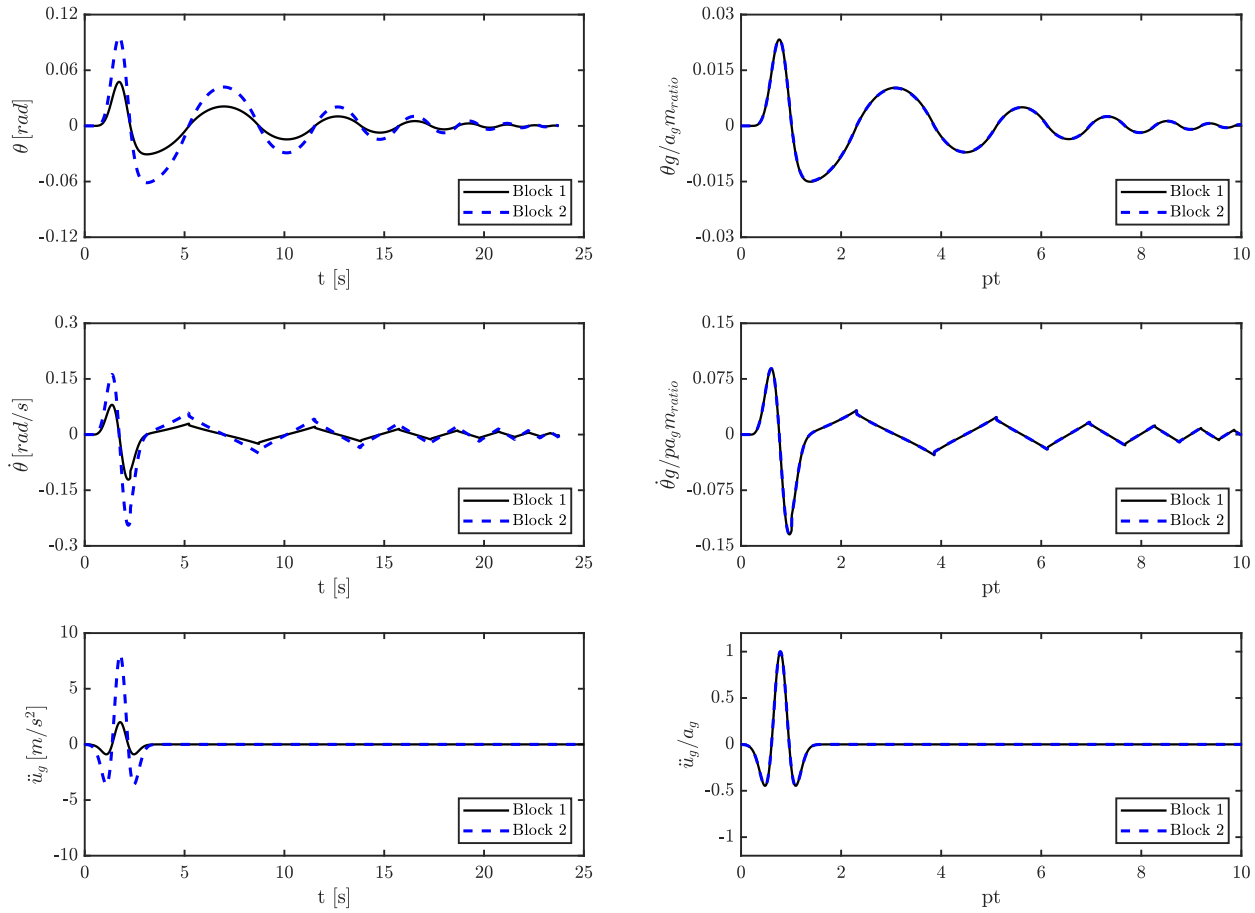

Figure 3: Response of two rocking structures of different shape and size but equivalent dimension-orientionless parameters (Block 1: $R_1 = 5[m]$, $\alpha_1 = 5°$ and $m_{ratio,1} = 10$; Block 2: $R_2 = 10[m]$, $\alpha_2 = 10°$ and $m_{ratio,2} = 5$). When the results are presented in dimension-orientionless terms both structures converge to a unique response.

where $T_g = 2\pi/\omega_g$ is the period that maximizes the Fourier spectrum of the symmetric Ricker wavelet, and a_g is the acceleration amplitude.

As noted in the previous section, the mass ratio has two competing effects on the dynamic response of the wall. On the one hand it reduces the frequency parameter, p_w, improving the global stability of the system (size effect of rocking behaviour[1]), while on the other hand it amplifies the ground acceleration. These effects can be examined with reference to Figure 4. Figure 4b shows the maximum rotation response of a given block ($R = 5[m]$ and $\alpha = 10°$) subjected to a symmetric Ricker pulse of acceleration amplitude $a_g = g \tan\alpha$ and frequency $\omega_g = 2.8[rad/s]$ for different values of mass ratio. The path followed by the block on the frequency ratio-acceleration amplitude plane is indicated with a white dashed line in Figure 4a.

The low mass ratio area of the spectrum shown in Figure 4b (or low frequency ratio according to Equation 4) show that small increments in the seismic mass cause the response to swiftly change from no-uplifting to overturning. As the mass ratio keeps increasing, the shift in the frequency parameter, p_w, takes the block outside of the overturning regions (indicated in blue and red in Figure 4a) and into the safe rocking

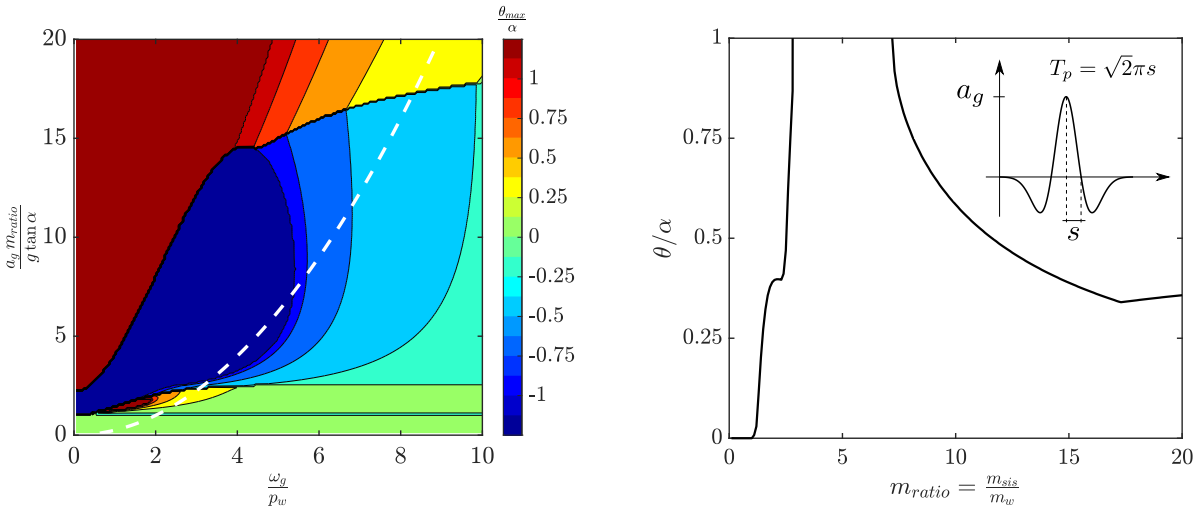

(a) Rocking spectrum for $\alpha = 10°$.

(b) Effect of m_{ratio} for a given block.

Figure 4: Effect of increasing m_ratio in the dynamic response of a rocking structure subjected to Ricker pulse ground motions. The white line in a) describes the path followed by the system in the rocking spectra.

area. The maximum rotation response then keeps decreasing until it starts surging again in the high mass ratio region (or high frequency ratio), although without reaching the overturning condition. In real rocking building structures, the mass ratio usually ranges from 1 (Housner's rocking block) to well over 10 in cases where the rocking element is only used as a lateral resistant system and the gravity loads are supported by secondary elements.

3. Dynamics of post-tensioned rocking systems

In post-tensioned rocking walls, the structural member is free to uplift and rock while post-tensioned tendons are incorporated to increase the lateral resistance and recentering capabilities of the building. Additional energy dissipation can be introduced by adding unbounded steel bars or external dissipation devices. This type of structures can be studied considering the model presented in Figure 5, where the rocking structure analysed in the previous section has been connected to the base through an elastic tendon passing through its middle. When the system of Figure 5 rotates the weight, W, and the force in the vertical tendon, F_{pt}, exert a restoring moment, M_r.

The post-uplifting stiffness of a free-standing wall (as the one studied in Section 2) is negative, since the line of action of the weight approaches the pivot point as rotation increases, reducing the lever arm of the restoring moment. By contrast, when elastic tendons are incorporated, the rotation of the wall increases the recentering elastic force, providing a positive stiffness that is added to the negative stiffness of the rocking block. The elongation of the tendon ,e, can be expressed as a function of the rotation θ (Figure 5):

$$e = R \sin\alpha \sqrt{2} \sqrt{1 - \cos\theta} \tag{9}$$

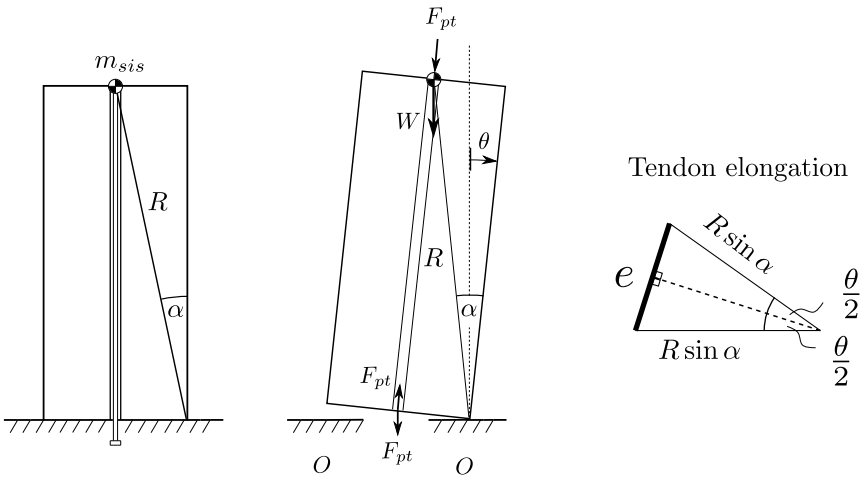

Figure 5: Post-tensioned rigid rocking structure under a horizontal ground excitation. The relation between base rotation and tendon elongation is also illustrated.

and the force in the post-tensioned tendon is:

$$F_{pt} = \frac{EA\,e}{R\cos\alpha} + P_0 = EA\tan\alpha\sqrt{2}\sqrt{1-\cos\theta} + P_0 \tag{10}$$

where $EA/R\cos\alpha$ is the axial stiffness of the vertical tendon and P_0 is the initial post-tensioning force. For a positive rotation ($\theta > 0$), the total restoring moment is given by:

$$M_r(\theta) = WR\sin(\alpha-\theta) + F_{pt}\,R\sin\alpha\cos\frac{\theta}{2} \tag{11}$$

Replacing Equation 10 into Equation 11 yields:

$$M_r(\theta) = WR\sin(\alpha-\theta) + R\sin\alpha\left(EA\tan\alpha\,\sin\theta + P_0\sqrt{\frac{1+\cos\theta}{2}}\right) \tag{12}$$

which can be rearranged as:

$$\frac{M_r(\theta)}{WR} = \sin\alpha\left(\cos\theta + \frac{P_0}{W}\sqrt{\frac{1+\cos\theta}{2}} + \sin\theta\left(\frac{EA}{W}\tan\alpha - \cot\alpha\right)\right) \tag{13}$$

If small rotations are considered (small θ), Equation 13 can be linearized such that:

$$\frac{M_r(\theta)}{WR} = \sin\alpha\left(1 + \frac{P_0}{W} + \theta\left(\frac{EA}{W}\tan\alpha - \cot\alpha\right)\right) \tag{14}$$

The term multiplying θ in Equation 14 corresponds to the stiffness of the system after uplifting. Therefore, the linearized condition to obtain a positive post-uplift stiffness is:

$$\frac{EA}{W} > \frac{1}{\tan^2\alpha} \tag{15}$$

This condition is equivalent to the expression obtained by Vassiliou and Makris [13] for vertically restrained classic rocking blocks. Figure 6 compares the moment-rotation response of post-tensioned rocking walls for different levels of normalized elastic force (EA/W) and initial post-tension force (P_0/W). As expected, the axial stiffness of the tendon only modifies the slope of the response after uplifting. On the other hand, the initial post-tensioning force increases the uplift threshold and therefore shifts the curves in Figure 6b vertically.

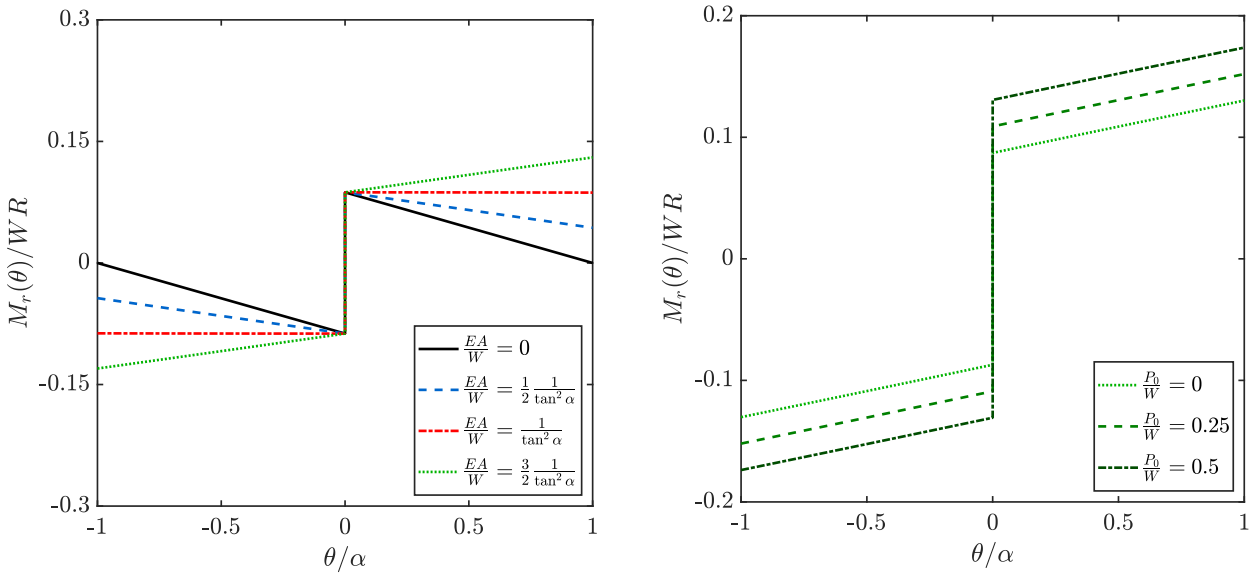

(a) No initial pre-stress ($P_0/mg = 0$).

(b) Constant tendon stiffness: $\frac{EA}{mg} = \frac{3}{2}\frac{1}{\tan^2\alpha}$.

Figure 6: Effect of a) the tendon stiffness, EA/W, and b) initial post-tensioning force, P_0/W, on the moment rotation relation of the rocking wall.

When m_{sis} crosses the pivot point a free-standing system becomes unstable. However, quick changes in the base acceleration may force the block back to a stable rocking position. Accordingly, overturning is only defined when the rotation response reaches an arbitrarily large value ($\theta \approx 90°$). On the other hand, the introduction of the post-tensioning increases the stiffness of the uplifted system, displacing the stability limit to higher rotations. If the post-uplift stiffness reaches a non-negative value, the system becomes, theoretically, unconditionally stable. In real applications, however, the capacity of the structure will be defined by the yield strength of the rocking surface and the post-tensioned tendons."

3.1. Free vibrations response of post-tensioned rocking systems

With reference to Figure 5, the evaluation of the rotational equilibrium about the rocking pivot point gives:

$$m_{sis}\, R^2\, \ddot{\theta} + WR\, \sin(\alpha - \theta) + R\, \sin\alpha \left(EA \tan\alpha\, \sin\theta + P_0 \sqrt{\frac{1+\cos\theta}{2}} \right) = 0 \qquad (\theta > 0) \qquad (16)$$

Introducing the frequency parameter, $p_w = \sqrt{g/R\,m_{ratio}}$, and rearranging leads to:

$$\ddot{\theta} = -p_w^2 \left(\sin(\alpha - \theta) + \sin\alpha \left(\frac{EA}{W} \tan\alpha \sin\theta + \frac{P_0}{W} \sqrt{\frac{1+\cos\theta}{2}} \right) \right) \tag{17}$$

Equation 17 can be linearized if slender blocks are considered ($\alpha \leq 20°$), such that:

$$\ddot{\theta} - p_w^2 \left(1 - \frac{EA}{W}\alpha^2 \right)\theta = -p_w^2 \alpha \left(1 + \frac{P_0}{W} \right) \tag{18}$$

If the post-uplift stiffness of the wall is null ($EA\alpha^2/W = 1$), the second term of the left-hand side of Equation 18 becomes zero, as the restoring moment is independent from the rotation amplitude. Therefore, for a wall released from rest ($\dot{\theta}(0) = 0$) with an initial rotation θ_0, the solution of Equation 18 is defined by parts as:

$$\theta(t) = \begin{cases} \frac{\alpha\left(1+\frac{P_0}{W}\right)}{1-\frac{EA}{W}\alpha^2} - \left(\frac{\alpha\left(1+\frac{P_0}{W}\right)}{1-\frac{EA}{W}\alpha^2} - \theta_0 \right) \cosh\left(p_w\, t \sqrt{1 - \frac{EA}{W}\alpha^2} \right) & \left(EA\alpha^2/W \neq 1\right) \\ \frac{-\alpha^2\, p_w\, t^2 \left(1+\frac{P_0}{W}\right)}{2} + \theta_0 & \left(EA\alpha^2/W = 1\right) \end{cases} \tag{19}$$

Equation 19 describes the motion of the wall as it rotates back to the vertical position. If there is no energy dissipation during impact, the block will then rotate in the negative direction ($-\theta$) reaching a maximum amplitude of $-\theta_0$, and fall back to reach its initial position. The time required to complete this cycle of oscillation is the period of free vibration. Following Housner's [1] reasoning, the time needed to go from $\theta = \theta_0$ to $\theta = 0$ corresponds to T/4. Therefore:

$$Tp_w = \phi\left(\frac{\theta_0}{\alpha}, \frac{EA\alpha^2}{W}, \frac{P_0}{W} \right) = \begin{cases} \frac{4}{\sqrt{1-\frac{EA}{W}\alpha^2}} \cosh^{-1}\left\{ \frac{1}{1-\frac{\theta_0\left(1-\frac{EA}{W}\alpha^2\right)}{\alpha\left(1+\frac{P_0}{W}\right)}} \right\} & \left(EA\alpha^2/W \neq 1\right) \\ 4\sqrt{\frac{2\,\theta_0}{\alpha\left(1+\frac{P_0}{W}\right)}} & \left(EA\alpha^2/W = 1\right) \end{cases} \tag{20}$$

Equation 20 shows that for a post-tensioned block of a given mass ratio and geometry (p_w and α), the period of oscillation, T, depends on the initial rotation, θ_0, the dimensionless elastic force, EA/W, and the dimensionless post-tension force, P_0/W. Figure 7 plots this expression for fixed values of θ/α, P_0/W and $EA\alpha^2/W$. As expected, Figure 7a shows that the period of oscillation decreases for higher values of initial post-tension and elastic forces. This effect is more significant closer to the origin ($P_0/W \leq 2$ and $EA\alpha^2/W \leq 1$) and becomes less important for higher values of vertical forces. On the other hand, Housner's early study already identified that the period of oscillation of a rocking body strongly depends on the initial

rotation amplitude[1]. The plots presented in Figure 7b and Figure 7c are consistent with this finding, showing that higher values of θ_0/α correspond to longer periods of oscillation. Moreover, the influence of the post-tensioned tendon is more important for initial rotations close to α, and becomes insignificant for small values of θ_0/α.

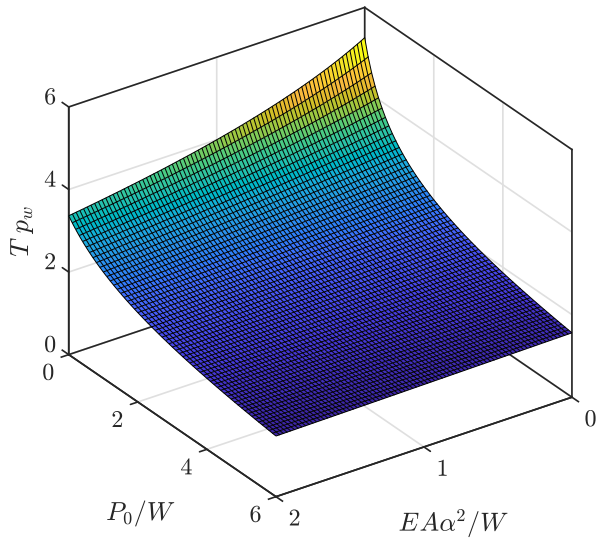

(a) Initial rotation, $\theta_0/\alpha = 0.5$.

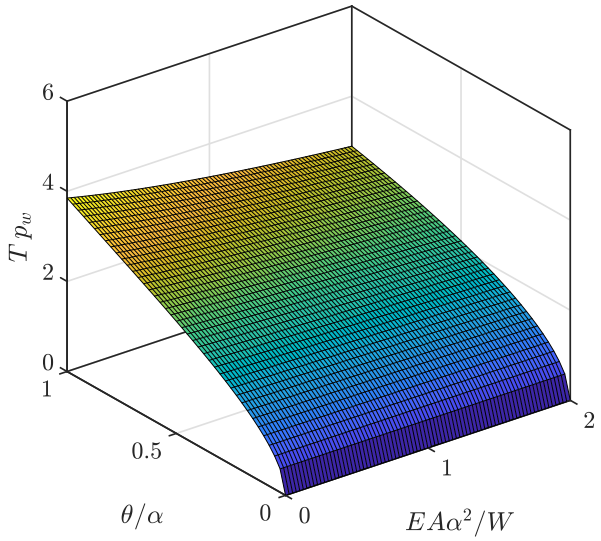

(b) Post-tensioning force $P_0/W = 2$.

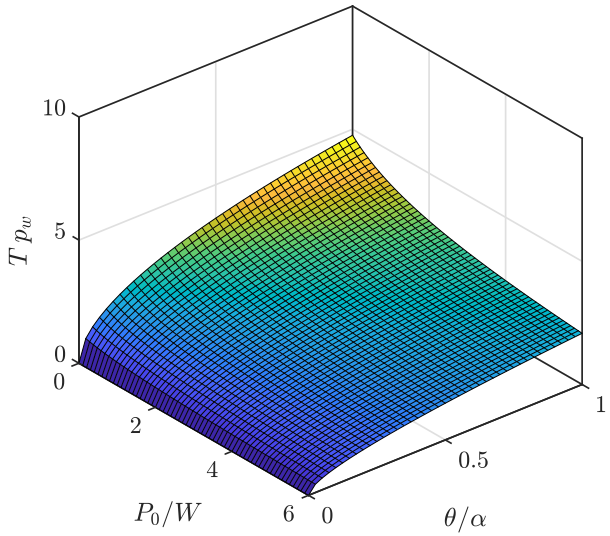

(c) Elastic force $EA\alpha^2/W = 1.5$ (positive stiffness after uplifting).

Figure 7: Effect of the initial rotation (θ/α), elastic force (EA/mg), and initial post-tensioning force (P_0) on the period of oscillation of a post-tensioned rocking structure.

3.2. Seismic response of post-tensioned structural walls

When subjected to a horizontal ground excitation, $\ddot{u}_g$, the post-tensioned rigid wall shown in Figure 5 uplifts and starts rocking when

$$\ddot{u}_g \geq \left(\frac{P_0}{W} + 1\right) \frac{g}{m_{ratio}} \tan\alpha \tag{21}$$

Evaluating the rotational equilibrium of the post-tensioned wall about the pivot points (positive and negative directions) gives:

$$m_{sis}\, R^2\, \ddot{\theta} + W R \sin(\alpha\, sgn(\theta) - \theta) + sgn(\theta)\, F_{pt}\, R \sin\alpha \cos\frac{\theta}{2} = -m_{sis}\, \ddot{u}_g R \cos(\alpha\, sgn(\theta) - \theta) \tag{22}$$

Combining Equations 10 and 22, and introducing the frequency parameter, $p_w = \sqrt{g/R\, m_{ratio}}$, yields:

$$\ddot{\theta} = -p_w^2 \left(\sin(\alpha\, sgn(\theta) - \theta) + m_{ratio} \frac{\ddot{u}_g}{g} \cos(\alpha sgn(\theta) - \theta) + \sin\alpha \left(\frac{EA}{W} \tan\alpha \sin\theta + sgn(\theta) \frac{P_0}{W} \sqrt{\frac{1+\cos\theta}{2}} \right) \right) \tag{23}$$

which is equivalent to the expression derived by Vassiliou and Makris [13] for vertically restrained rigid blocks. Again, this equation of motion can be linearized if slender walls are considered ($\alpha \leq 20°$), such that:

$$\ddot{\theta} = -p_w^2 \left(\alpha\, sgn(\theta) \left(1 + \frac{P_0}{W}\right) + \theta \left(\frac{EA\alpha^2}{W} - 1 \right) + m_{ratio} \frac{\ddot{u}_g}{g} \right) \tag{24}$$

Figure 8 compares the seismic demands (peak rotation and angular acceleration) for slender walls with different levels of elastic and initial post-tensioning force, subjected to symmetric Ricker pulses of acceleration amplitude $a_g = 2\, g \tan\alpha / m_{ratio}$. The analyses presented in Figure 8 consider dimensionless elastic forces that result in post-uplifting stiffnesses varying from negative to positive values, while the maximum post-tensioning force is limited by the rocking-triggering condition (Equation 21). The response of a free-standing rocking block is also included in Figure 8 for comparative purposes.

The results depicted in Figure 8 show that the elastic force improves the stability of the wall when $\omega_g / p_w < 2$ (small structures), but has very little effect on the maximum rotation and acceleration response for larger structures. This behaviour is related to the increase in the post-uplifting stiffness, which allows the block to withstand rotations greater than α and still return to its vertical position. Nevertheless, higher rotational accelerations are observed for some small to medium-sized structures ($\omega_g / p_w < 4$) in comparison with free-rocking systems. Moreover, the larger the elastic force the higher the relative acceleration at lower frequency ratios ($\omega_g / p_w < 4$).

On the other hand, the level of initial post-tensioning force has a more significant effect on the maximum rotation response of both, small and large structures. While an improved stability can be observed for $\omega_p / p < 4$, reductions in the maximum rotations for greater frequency ratios (larger walls) are also obtained. Importantly, the response enhancement becomes more significant the higher the level of initial post-tensioning. However, these improvements happen at the expense of inducing higher rotational accelerations over the full range of frequency ratios studied.

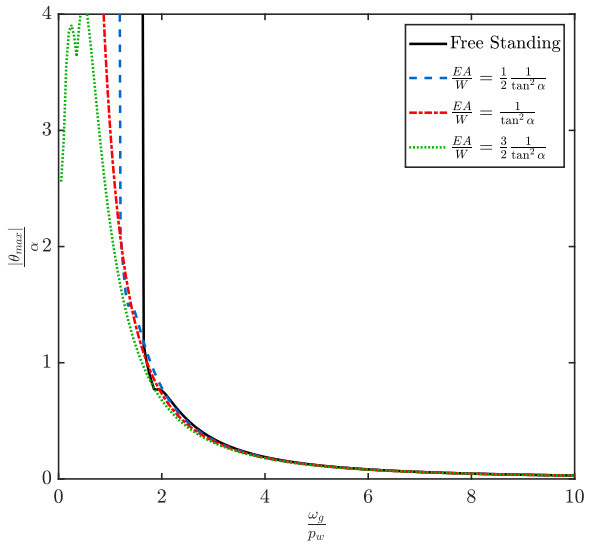

(a) Rotation spectra, $P_0 = 0$.

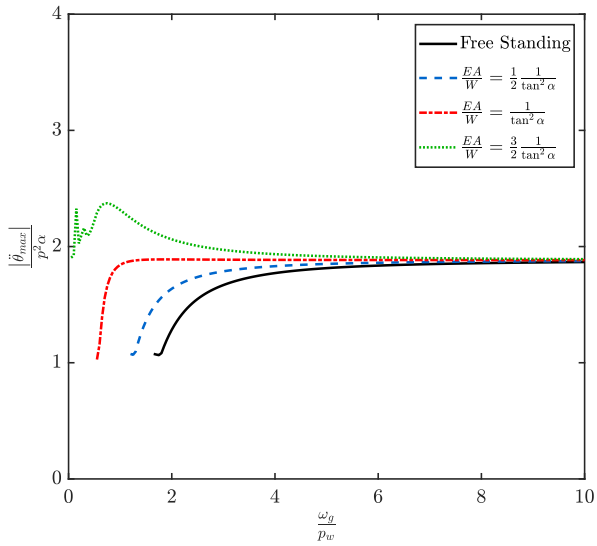

(b) Acceleration spectra, $P_0 = 0$.

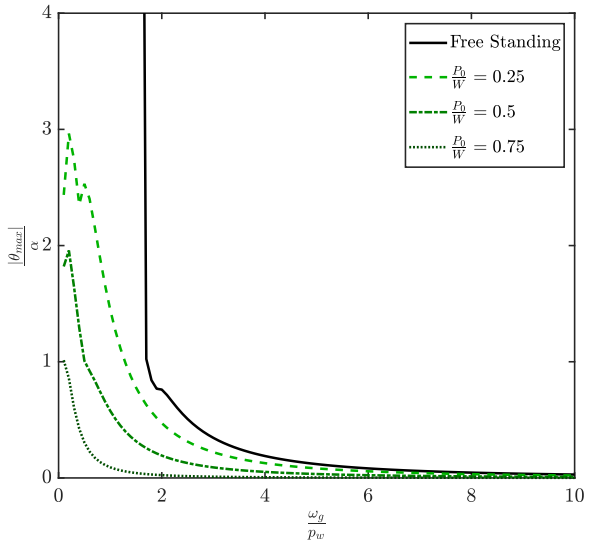

(c) Rotation spectra, $\frac{EA}{W} = \frac{3}{2}\frac{1}{\tan^2\alpha}$.

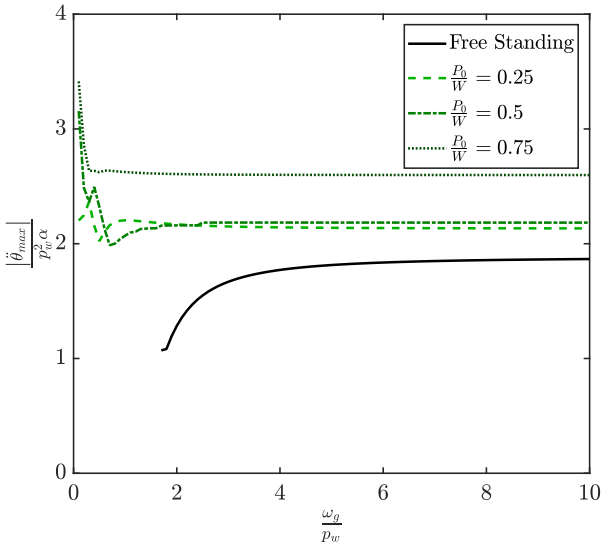

(d) Acceleration spectra, $\frac{EA}{W} = \frac{3}{2}\frac{1}{\tan^2\alpha}$.

Figure 8: Effect of the dimensionless elastic force, EA/W, and dimensionless initial post-tensioning force, P_0/W, on the rotation and angular acceleration demands for slender walls subjected to Ricker pulses of acceleration amplitude $a_g = 2\,g\,\tan\alpha/m_{ratio}$.

The results presented in Section 2.1 show that regardless of the acceleration amplitude of a ground motion, the intensity dimensionless parameter, $a_g m_{ratio}/g\tan\alpha$, can be significantly amplified by the ratio between the seismic and gravitational masses. Consequently, high effective acceleration amplitudes that are usually not relevant for the study of classic free-standing blocks, need to be considered when dealing with post-tensioned rocking building structures.

Figure 9 compares the peak seismic demands (rotation and angular acceleration) for different post-tensioned rocking structures subjected to acceleration pulses of amplitude $a_g = 20\,g\tan\alpha/m_{ratio}$. The

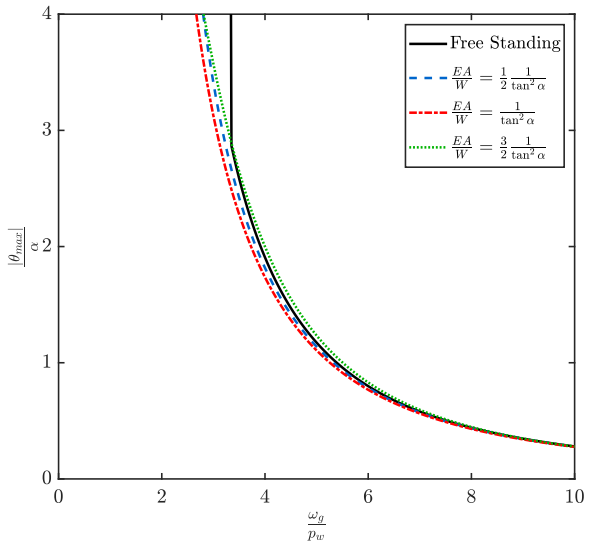

(a) Rotation spectra, $P_0 = 0$.

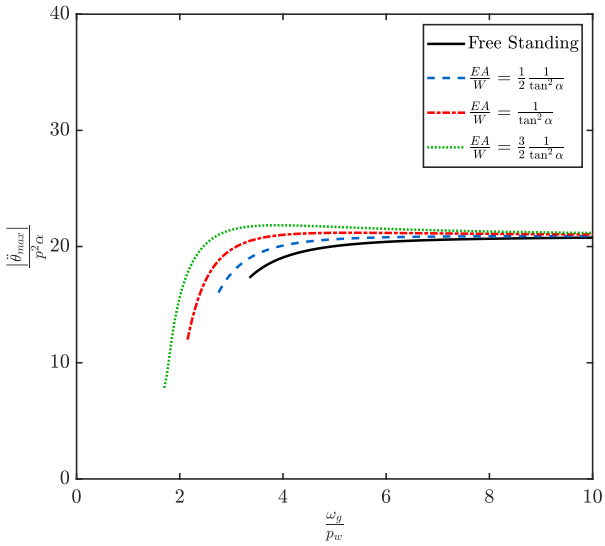

(b) Acceleration spectra, $P_0 = 0$.

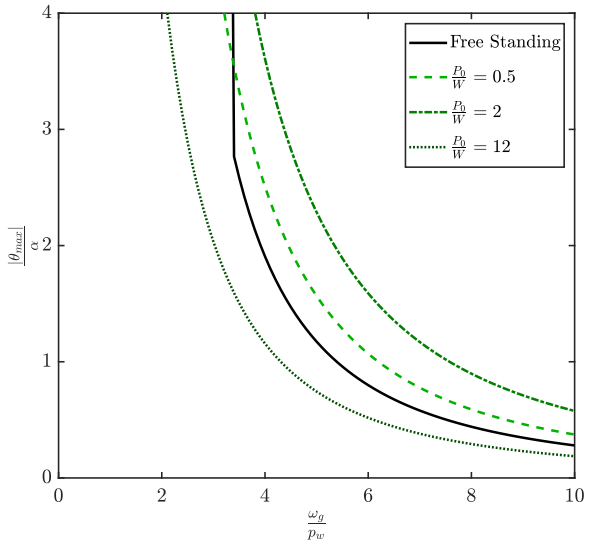

(c) Rotation spectra, $\frac{EA}{W} = \frac{3}{2}\frac{1}{\tan^2\alpha}$.

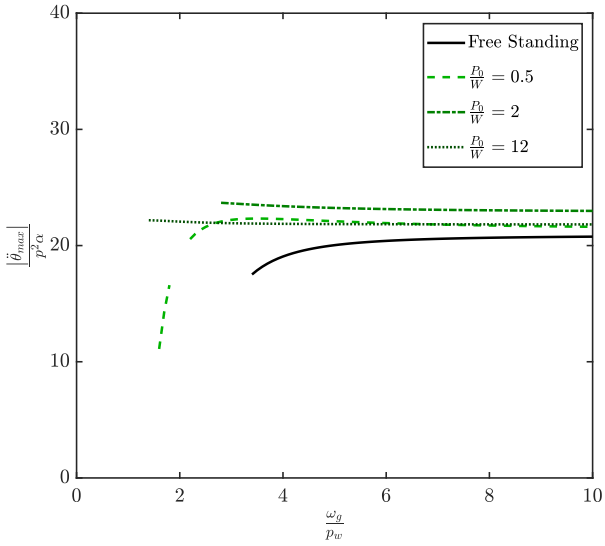

(d) Acceleration spectra, $\frac{EA}{W} = \frac{3}{2}\frac{1}{\tan^2\alpha}$.

Figure 9: Effect of the dimensionless elastic force, EA/W, and dimensionless initial post-tensioning force, P_0/W, on the peak rotation and angular acceleration demands for slender walls subjected to Ricker pulses of acceleration amplitude $a_g = 20\,g\,\tan\alpha/m_{ratio}$.

results of the analyses suggest that the use of post-tensioned tendons becomes less advantageous when pulses of higher acceleration amplitude are considered. Although the elastic force slightly reduces the overturning cases, the initial post-tensioning force can increase the rotation and acceleration demands in some cases. This behaviour is studied in more detail in Figure 10, where the maximum response of a block with $\omega_p/p_w = 4$ to symmetric Ricker pulses of different acceleration amplitude is plotted as a function of the dimensionless initial post-tensioning force.

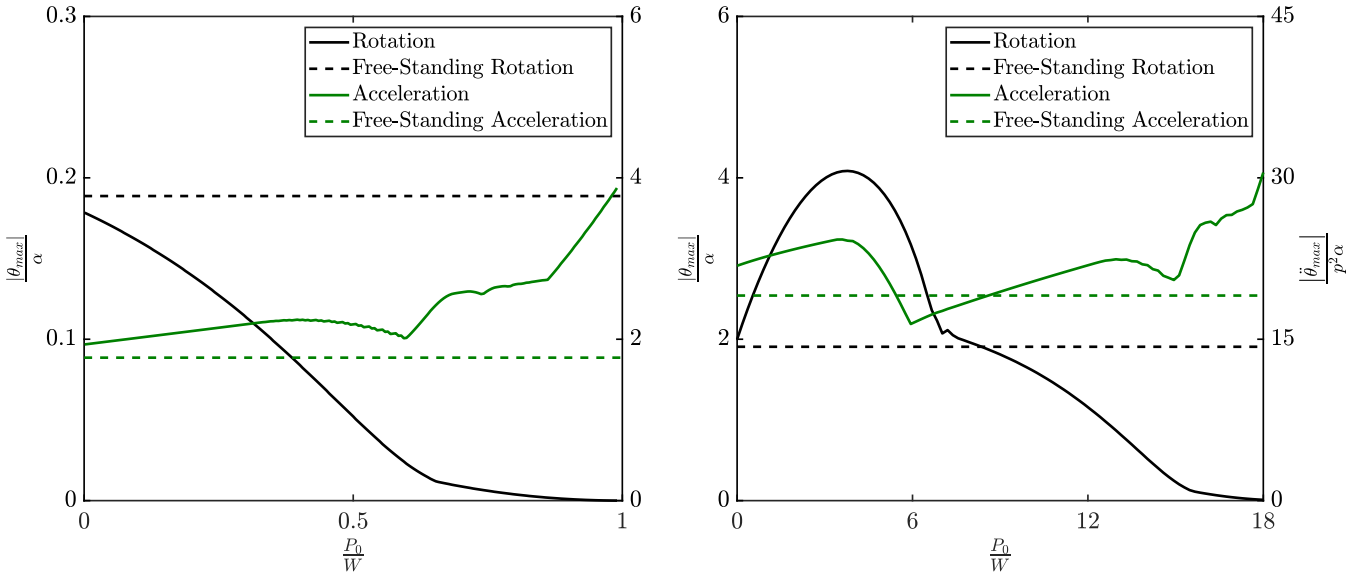

(a) $a_g = 2\,g\,\tan\alpha/m_{ratio}$. (b) $a_g = 20\,g\,\tan\alpha/m_{ratio}$.

Figure 10: Effect of the dimensionless initial post-tensioning force, P_0/W, on the rotation and angular acceleration demands of a slender wall subjected to a symmetric Ricker pulse of frequency ratio $\omega_p/p_w = 4$.

It can be observed from Figure 10a that for low ground acceleration amplitudes, larger initial post-tensioning forces are related to proportionally lower maximum rotations with the potential to suppress the rocking response altogether (Equation 21). As previously observed in Figure 8, this reduction is accompanied by an important increase in the maximum peak accelerations. For the post-tensioned wall considered in the analysis ($\alpha \leq 20°$, $\omega_p/p_w = 4$) and with reference to the response of a free-standing block, a reduction of 50% in the maximum rotation would be associated with a 25% increase in the peak angular acceleration. This acceleration magnification becomes even more significant for higher levels of initial post-tensioning force.

On the other hand, when ground motions of higher acceleration amplitudes are considered (Figure 10b), a spectral region where the rotation and acceleration are simultaneously amplified can be identified. For small values of dimensionless initial post-tensioning force ($P_0/W < 6$), rotation demands are significantly amplified, reaching a peak of more than twice the maximum rotation of the benchmark free-standing block at around $P_0/W \approx 4$. A similar trend is observed for rotational acceleration demands, although with a smaller amplification ratio. This observation is particulary relevant, as it happens at levels of initial post-tensioning force ratios that are most commonly observed in practice. For higher magnitudes of initial post-tensioning forces, the behaviour of the seismic demands resembles the trends observed in Figure 10a for smaller ground acceleration amplitudes, with maximum rotations reducing progressively and peak accelerations being amplified.

4. Seismic control of post-tensioned walls with inerters

Although post-tensioned systems have been shown to be effective in controlling structural damage, high rotations and accelerations associated with the rocking motion can cause significant non-structural and con-

tents damage. Previous analyses conducted on free-rocking bodies[34] showed that the use of supplemental rotational inertia can help to significantly reduce their seismic demands. This control strategy can also be applied to post-tensioned walled buildings by connecting the inerter directly to the rocking elements or rigid diaphragm of the structure, as shown in Figure 11. For low-rise buildings, the wall element can be assumed to behave as a rigid block, and the dynamic behaviour of the system can be studied simply incorporating the contribution of the inerter to the models examined in previous sections. Herein, an inerter connected to the top of the wall (Point C) is considered for simplicity.

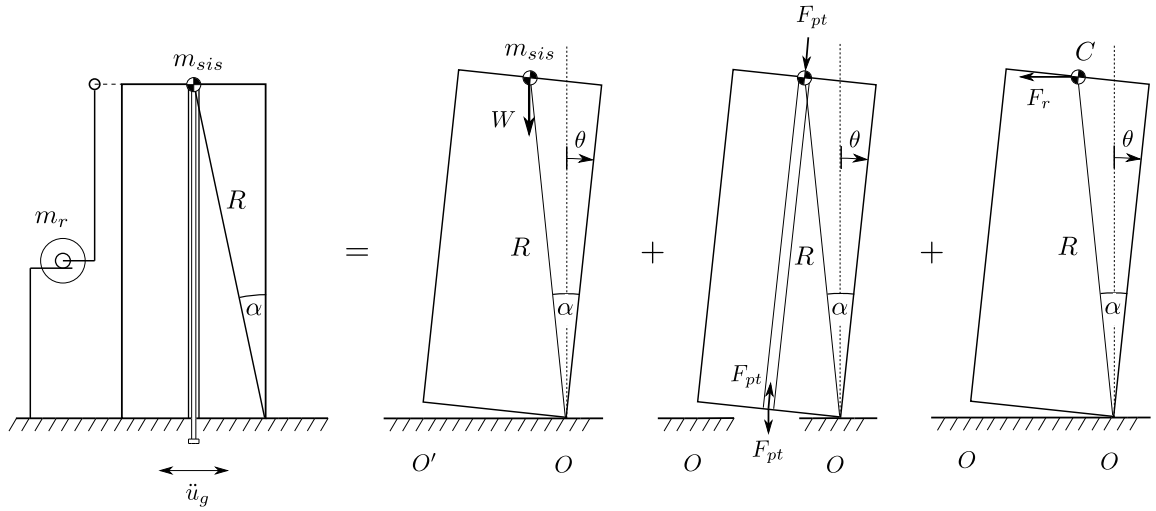

Figure 11: Single-degree-of-freedom system representing a post-tensioned rocking wall connected to a grounded inerter of apparent mass m_r. The system can be studied combining the effects of the seismic mass and gravitational loads, the post-tensioned tendon and the inerter device.

Rocking motion initiates when the overturning moment due to the ground excitation exceeds the restoring moment exerted by the self-weight and the vertical tendon (Equation 21). Until this instant, the resisting force in the inerter is zero, since there is no relative acceleration between its terminals. Once the block uplifts, point C in Figure 11 follows a circular path. Neglecting the contribution of the centripetal acceleration, the resisting force in the inerter is:

$$F_r = m_r \, R \, \ddot{\theta} \cos(\alpha sgn(\theta) - \theta) \tag{25}$$

where m_r is the inertance or apparent mass of the inerter. Evaluating the rotational equilibrium around the rocking pivot point gives:

$$\begin{aligned} \big(m_{sis}R^2 \, + m_r R^2 \cos^2(\alpha \, sgn(\theta) - \theta)\big)\ddot{\theta} + \, WR \, \sin(\alpha \, sgn(\theta) - \theta) + sgn(\theta) \, F_{pt} \, R \, \sin\alpha \cos\frac{\theta}{2} \\ = -m_{sis} \, \ddot{u}_g R \, \cos(\alpha \, sgn(\theta) - \theta) \end{aligned} \tag{26}$$

Combining Equation 10 and Equation 26, and rearranging:

$$\ddot{\theta} = -p_{w,\sigma}^2 \left(\sin(\alpha\, sgn(\theta) - \theta) + m_{ratio}\, \frac{\ddot{u}_g}{g} \cos(\alpha sgn(\theta) - \theta) + \sin\alpha \left(\frac{EA}{W} \tan\alpha \sin\theta + sgn(\theta)\, \frac{P_0}{W} \sqrt{\frac{1+\cos\theta}{2}} \right) \right) \tag{27}$$

with

$$p_{w,\sigma} = \sqrt{\frac{g}{m_{ratio}\, R \left(1 + \sigma \cos^2(\alpha\, sgn(\theta) - \theta)\right)}} \tag{28}$$

where σ is the aparent mass ratio defined as: $\sigma = m_r/m_{sis}$. Equation 27 and Equation 28 are analogous to the equation of motion obtained by Thiers-Moggia and Malaga-Chuquitaype[34] for free-rocking bodies equipped with inerters. These expressions show that the inclusion of the inerter effectively reduces the frequency parameter, p_w, of the post-tensioned rocking element. This reduction generally results in enhanced stability and lower seismic demands due to the well-known size effect of the rocking behaviour[1]. Importantly, the frequency parameter of a rocking wall depends only on the size, R, and the mass ratio of the structure (Equation 4). Consequently, it cannot be modified without altering the elevation (R) or the plan distribution of the building (m_{ratio}). This highlights the significance of inerter-based control strategies as they open the door for an expedient modification of the dynamic response of a rocking system without altering its geometry.

As mentioned previously, in most practical cases the wall elements can be considered to be slender ($\alpha < 20°$), and Equation 27 can be linearized such that:

$$\ddot{\theta} = -p_{w,\sigma}^2 \left(\alpha\, sgn(\theta) \left(1 + \frac{P_0}{W}\right) + \theta \left(\frac{EA\alpha^2}{W} - 1 \right) + m_{ratio}\, \frac{\ddot{u}_g}{g} \right) \tag{29}$$

with

$$p_{w,\sigma} = \sqrt{\frac{g}{m_{ratio}\, R\, (1+\sigma)}} \tag{30}$$

4.1. Structural demands under single pulse excitations

In order to thoroughly assess the effectiveness of the proposed system, the response of a wide range of post-tensioned rocking structures subjected to symmetric Ricker pulses was examined. Walls of positive post-uplift stiffness ($EA/W = 3/2 \tan^2\alpha$) and initial post-tensioning force equal to $P_0/W = 5$ are selected as representative of typical design configurations. Additionally, two apparent mass ratios, $\sigma = 0.5$ and $\sigma = 1$, are considered for the structures equipped with inerters. It is important to note that, although the apparent mass ratios are relatively high, the actual gravitational masses can be kept several orders of magnitude lower by using amplifying mechanisms such as ball-screws[42] or geared wheels[21]. The results presented below correspond to acceleration pulses with amplitude $a_g = 9\, g\, \tan\alpha / m_{ratio}$, representing to 1.5 times the amplitude required to trigger the rocking motion (Equation 21).

Figure 12 presents the results of the analyses in terms of rotation and acceleration spectra. As noted above, the introduction of post-tensioning reduces the maximum rotation of the walls, although in this case

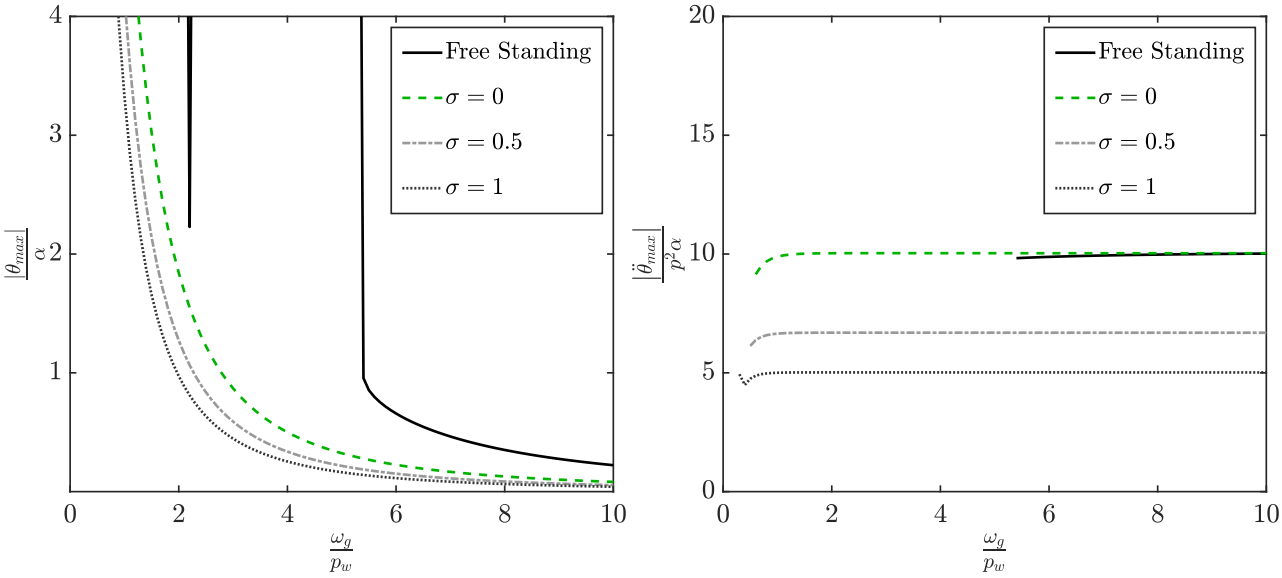

(a) Rotation spectra.

(b) Acceleration spectra.

Figure 12: Peak rotation and acceleration demands in post-tensioned rocking structures of positive post-uplift stiffness ($EA/W = 3/2 \tan^2\alpha$) and initial force $P_0/W = 5$, with and without inerters, subjected to symmetric Ricker pulses of acceleration amplitude $a_g = 9\,g\,\tan\alpha/m_{ratio}$.

it has a negligible effect on the acceleration demands. The inerter on the other hand, further reduces the peak rotations while at the same time it significantly diminishes the angular accelerations. Moreover, while the reduction in rotations becomes less significant for higher frequency ratios, the decrease in accelerations is almost constant along all frequency ratios, reaching reductions of around 50% for $\sigma = 1$.

Another parameter of great interest for the seismic design of post-tensioned buildings is the base shear, V_b. Considering that the slender wall element behaves approximately as a rigid block, this can be obtained as:

$$V_b(\theta) = \frac{M_r(\theta)}{R} \tag{31}$$

where M_r is the restoring moment exerted by the weight, W, and the post-tensioned tendon. Figure 13a shows the base shear corresponding to the same structures analysed above. As expected, for the case of negative stiffness (free-standing wall), the maximum shear force is constant and determined by the uplifting condition. The introduction of the initial post-tensioning force significantly increases this lower limit (Equation 21), amplifying also the base shear of the post-tensioned structures. Since the positive stiffness of the rocking walls is relatively low, the reduction in rotations brought about by the inerter does not translate in a significant reduction of the restoring moment, and therefore the base shear is mainly controlled by the uplift resistance.

This contrasts with previous studies conducted on fixed-base frames that found significant forces can develop in the inerter [29], which can limit the practical implementation of the system unless clutching is ensured[30]. Figure 13b shows the resisting force developed in the inerter for the protected structures under

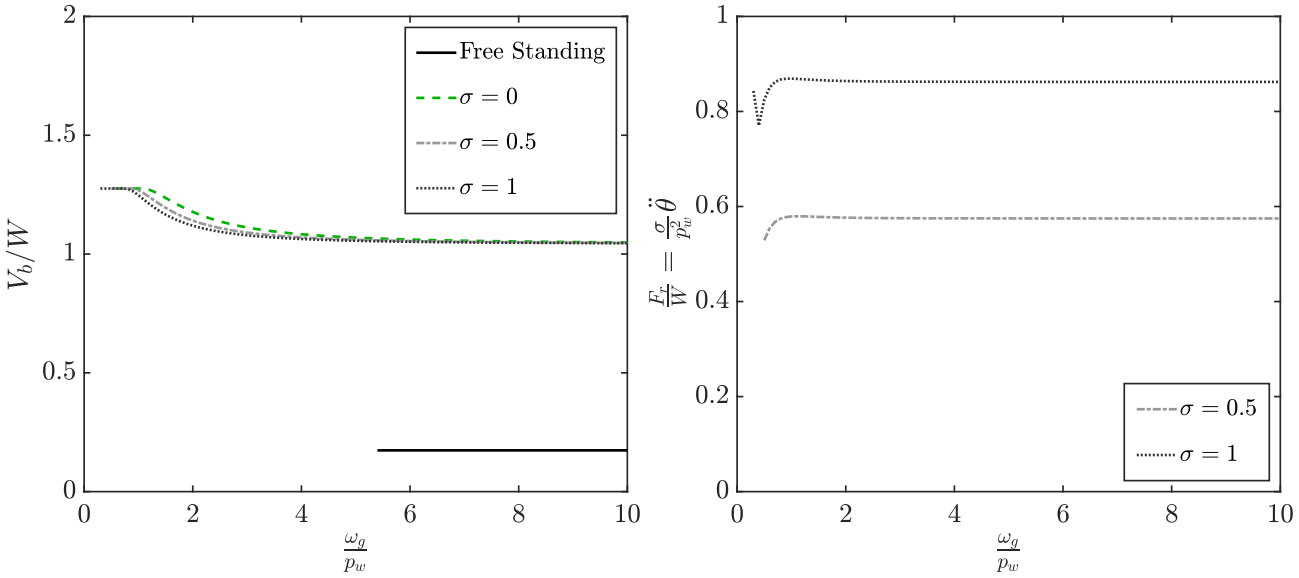

(a) Normalized base shear.

(b) Normalized force in the inerter.

Figure 13: Base shear and inerter force in post-tensioned rocking structures of positive post-uplift stiffness ($EA/W = 3/2\tan^2\alpha$) and initial force $P_0/W = 5$, with and without inerters, subjected to symmetric Ricker pulses of acceleration amplitude $a_g = 9\,g\,\tan\alpha/m_{ratio}$.

consideration. Forces of around 58% and 85% of the weight supported by the wall, W, were registered for $\sigma = 0.5$ and $\sigma = 1$ respectively. Although this values can seem high, they are lower than the vertical post-tensioning load considered in the analyses, and therefore should be accommodated by adequate detailing.

4.2. Seismic demands under real pulse-like ground motions

In the previous section, the dynamic behaviour of post-tensioned rocking structures equipped with inerter devices was studied using single Ricker pulse excitations. In real seismic events, structures are subjected to an acceleration history that can be represented as a series of individual pulses with different frequencies. The early work of Housner [1] already identified that the action of these successive pulses can increase the structural demands and overturn free-standing blocks for smaller acceleration amplitudes than a single pulse excitation. In this section, the effectiveness of the inerter for the control of the seismic response of rocking structures is assessed. To this end, a set of 202 pulse-like ground motion records obtained from the Pacific Earthquake Engineering Research Center (PEER) database is employed. Records from 21 earthquakes with magnitudes Mw ranging from 5.4 to 7.9 are considered. Table 1 summarizes the catalogue of earthquakes used for the analyses [34]. Our study does not consider uncertainties related to the structural properties, since it is typically the case that the uncertainties associated with the ground-motion are more significant on the structural response [43, 44].

A 3-storey rigid-wall system ($R = 9[m]$ and $\alpha = 10°$) with positive post-uplift stiffness ($EA/W = 3/2\tan^2\alpha$), $m_{ratio} = 5$ and $P_0/W = 5$ was selected as a realistic case study, while an inerter of apparent mass ratio $\sigma = 1$ was considered. Figure 14 compares the rotation and acceleration response histories of the buildings subjected to the 90° component of the 1986 San Salvador earthquake. Three cases are assessed

Table 1: Ground motion database used in the analyses

Earthquake name	**Year**	**Magnitude M_w**	**Mechanism**	**Number of Records**
San Fernando	1971	6.61	Reverse	1
Tabas Iran	1978	7.35	Reverse	1
Coyote Lake	1979	5.74	Strike Slip	4
Imperial Valley-06	1979	6.53	Strike Slip	12
Irpinia Italy-01	1980	6.9	Normal	2
Westmorland	1981	5.9	Strike Slip	1
Morgan Hill	1984	6.19	Strike Slip	2
Kalamata Greece-02	1986	5.4	Normal	1
San Salvador	1986	5.8	Strike Slip	2
Superstition Hills-02	1987	6.54	Strike Slip	2
Loma Prieta	1989	6.93	Reverse Oblique	6
Cape Mendocino	1992	7.01	Reverse	1
Landers	1992	7.28	Strike Slip	3
Northridge-01	1994	6.69	Reverse	14
Kobe	1995	6.9	Strike Slip	4
Kocaeli	1999	7.51	Strike Slip	4
Chi-Chi Taiwan	1999	7.62	Reverse Oblique	36
Chi-Chi Taiwan-04	1999	6.2	Strike Slip	1
Chi-Chi Taiwan-06	1999	6.3	Reverse	2
Duzce Turkey	1999	7.14	Strike Slip	1
Denali Alaska	2002	7.9	Strike Slip	1
			Total	**202**

in this figure: i) a free-rocking building, ii) a building with a post-tensioned wall and iii) the same post-tensioned building equipped with an inerter of apparent mass $\sigma = 1$. The rotation is presented in radians whereas accelerations are presented as the linear acceleration at Point C (Figure 11), obtained as the product of the angular acceleration, $\ddot{\theta}$, and the size parameter of the wall, R- in g.

The results plotted in Figure 14 are consistent with the observations made in previous sections for single pulse excitations. The addition of the post-tensioned tendons reduced the maximum rotation of the wall but increased the peak acceleration. Nevertheless, the introduction of the inerter efficiently offsets this effect, further diminishing the rotation response and significantly reducing accelerations to levels even lower than those of the benchmark free-standing structure.

A cloud analysis considering the earthquake database described in Table 1 was conducted in order to compare the seismic performance of the post-tensioned structures with and without inerters. The uniform duration, t_{uni}, which corresponds to the sum of the time intervals during which the ground acceleration exceeds the limit to cause uplifting (Equation 21), was selected as the intensity measure, as recommended by Dimitrakopoulos et al[45].

A common assumption in seismic demand models is to consider that the median estimated demand $\overline{D}_m$ and the intensity measure IM follow a power law [45, 46]

$$\overline{D}_m = a\, IM^b \tag{32}$$

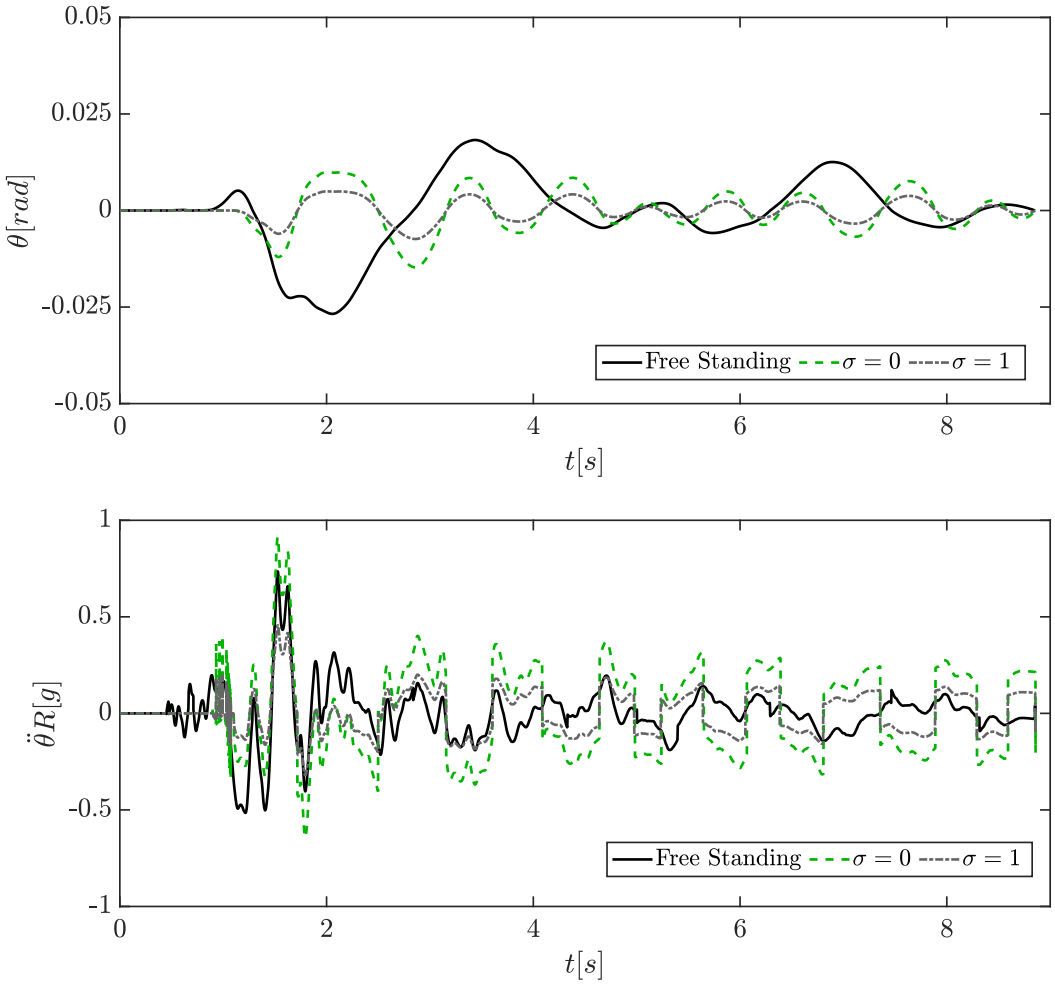

Figure 14: Rotation and acceleration response of a post-tensioned rocking structure of $R = 9[m]$, $\alpha = 10^{\circ}$, $m_{ratio} = 5$, positive post-uplift stiffness ($EA/W = 3/2 \tan^2 \alpha$) and $P_0/W = 5$, with and without inerters, subjected to the 90° component of the 1986 San Salvador earthquake.

When plotted on a $ln(\overline{D}_m) - ln(IM)$ plane, Equation 32 becomes a straight line

$$ln(\overline{D}_m) = ln(a) + b\, ln(IM) \tag{33}$$

where a and b are regression coefficients. Figure 15 presents the results of the cloud analysis and the corresponding fitted seismic demand models for the protected and unprotected structures. The results of the regression analyses show a strong correlation between the selected intensity measure, t_{uni}, and the seismic demands, validating the estimation model proposed in Equation 32.

In general, the structure equipped with inerter devices shows significantly smaller seismic demands for the whole range of IMs considered. Mean reductions of around 50% are observed in both peak rotations and peak accelerations (note the logarithmic scale). These conclusions are consistent with observations made in Figure 14 and the results obtained in Section 4.1 for single pulse excitations.

As discussed previously, post-tensioned systems have proved to be highly effective in controlling structural

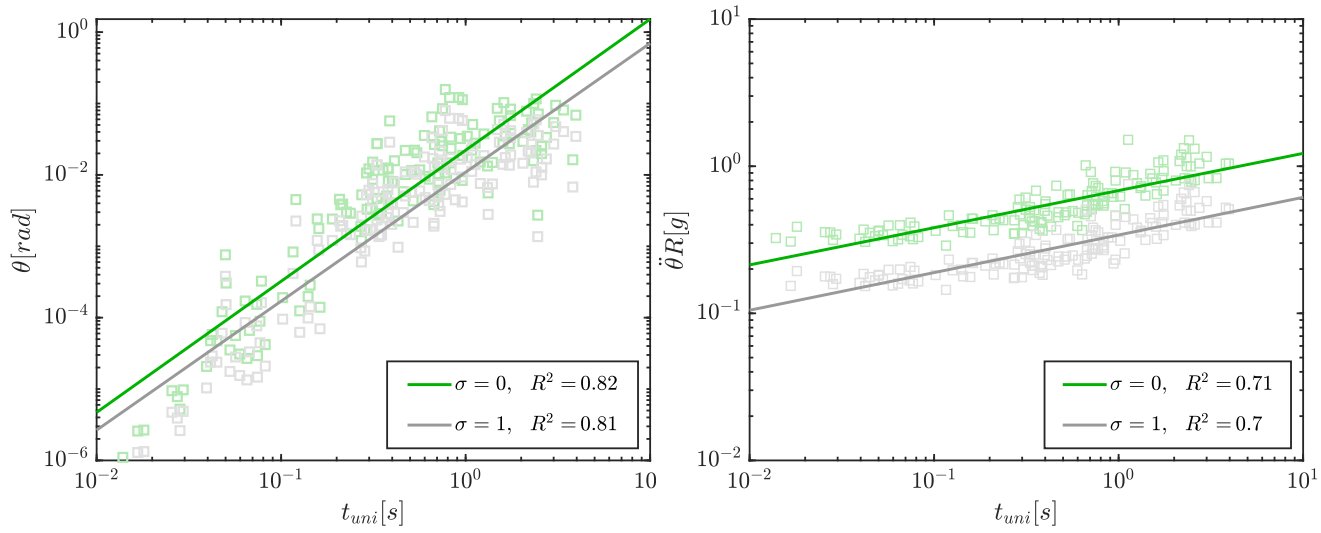

(a) Peak rotations.

(b) Peak accelerations.

Figure 15: Peak rotation and acceleration demands of post-tensioned rocking structures of $R = 9[m]$, $\alpha = 10°$, $m_{ratio} = 5$, positive post-uplift stiffness ($EA/W = 3/2 \tan^2 \alpha$) and $P_0/W = 5$, with and without inerters, subjected to the earthquake database shown in Table 1.

damage. Nevertheless, economic losses during seismic events are usually controlled by damage to non-structural components, which is often triggered at response intensities that are smaller than those required to produce structural damage[47]. Performance-based assessment of non-structural building components requires the identification of drift and acceleration sensitive elements and the definition of their corresponding limits[12]. Design codes typically specify these limits as a function of the non-structural component typology. With the aim of comparing the overall performance of post-tensioned walled structures with and without ineters, the limit defined in Eurocode 8 [48] for buildings having ductile non-structural components, $\theta \leq 0.75\%$, is adopted in this study. Figure 16a shows the fragility functions associated to this limit state obtained for the protected and unprotected structures considered in the previous analyses. The cloud-to-IDA procedure proposed by Miano et al.[49] was used to minimize the number of analyses and amount of scaling.

On the other hand, the design of acceleration-sensitive non-structural components traditionally entails the computation of floor response spectra[50]. Nonetheless, the peak floor acceleration can be used as a first proxy in order to assess the performance of the proposed seismic control strategy. Figure 16b presents the fragility functions associated to an acceleration limit of $R\ddot{\theta} = 0.5[g]$.

The fragility functions depicted in Figure 16 demonstrate the significant improvement in the performance of post-tensioned rocking structures brought about by the inerter. In terms of rotations, the estimated median IM associated with the selected drift limit state is $\tilde{t}_{uni} = 0.5[s]$ for the unprotected structure, whereas this parameter increases to $\tilde{t}_{uni} = 0.74[s]$ when the inerter is introduced. Moreover, the response enhancement becomes more important for higher probabilities of exceedance. Similar trends are observed in the case of peak floor accelerations, with an even greater increase (nearly four-fold) in the median IM. On the other hand, smaller variations were obtained on the logarithmic standard deviation, β_{lnX}. The results presented in Figure 16 are in line with the demand reductions observed in the previous sections and allow

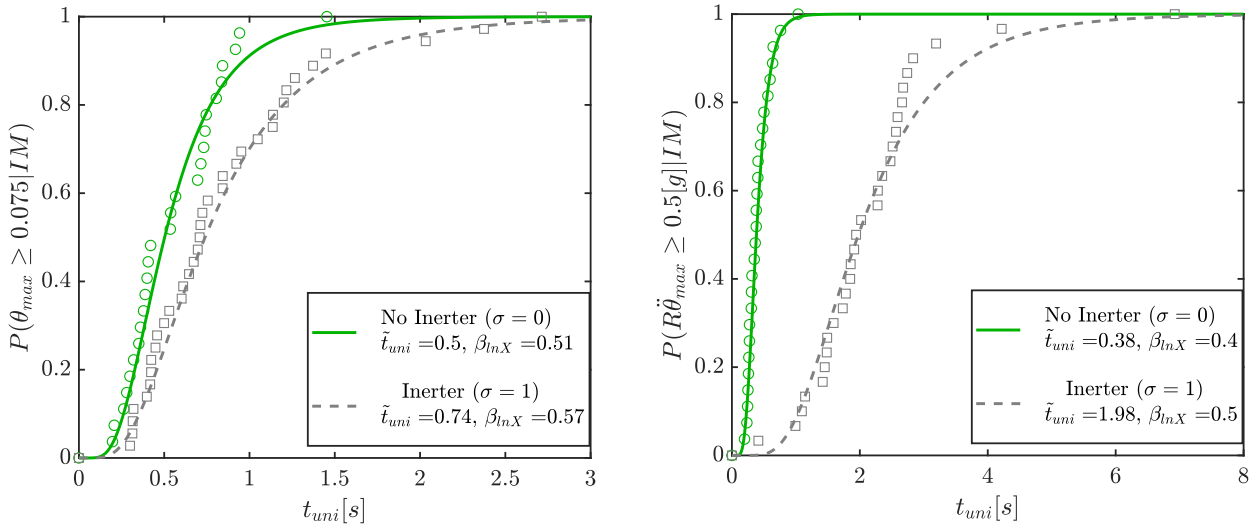

(a) Rotation limit: $\theta_{max} = 0.75\%$.

(b) Acceleration limit: $R\,\ddot{\theta}_{max} = 0.5[g]$.

Figure 16: Fragility functions for post-tensioned rocking structures of $R = 9[m]$, $\alpha = 10°$, $m_{ratio} = 5$, positive post-uplift stiffness ($EA/W = 3/2\tan^2\alpha$) and $P_0/W = 5$, with and without inerters.

us to conclude that the use of of supplemental rotational inertia devices configures a practical alternative to improve the dynamic response and boost the overall seismic performance of rocking building structures.

5. Conclusions

In this paper we have examined the basic dynamic behaviour of post-tensioned rocking structures and assessed the feasibility of using supplemental rotational inertia to reduce their structural demands and improve their overall seismic performance. Firstly, a modified rigid block representative of rocking building structures was defined. Importantly, our model considers the possibility of having different seismic and gravitational masses through the introduction of an m_{ratio} parameter. Based on a formal dimensional-orientational assessment of the system, we have demonstrated that this mass ratio can be incorporated into the existing Π-parameters without introducing a new dimensionless group.

In a second stage, a vertical post-tensioned tendon was introduced to the model. After deriving the equations of motion, we examined the free-vibration response of the system. Additionally, the structural demands under Ricker pulse excitations were studied in terms of maximum rotations and peak angular accelerations. The results of these analyses showed that the elastic force can help to improve the stability of smaller rigid blocks, but has little effect on larger structures. This behaviour is related to the increase in the post-uplift stiffness which allows the block to survive rotations greater than its slenderness, α, and still return to the vertical position. On the other hand, the initial post-tensioning force had a more significant effect on the maximum rotations of both, smaller and larger structures. Moreover, the improvement in the response becomes more important the higher the level of initial force. Nevertheless, these rotation reductions are accompanied by a significant increase on the peak angular accelerations at low frequency ratios for unstressed rocking structures and over the full spectral range in the case of structures with non-zero levels of initial post-tensioning.

The introduction of the mass ratio parameter, m_{ratio}, implies that regardless of the acceleration amplitude of a ground motion, the intensity dimensionless parameter, $a_g m_{ratio}/g \tan\alpha$, can assume significantly high values. Consequently, the consideration of high effective acceleration amplitudes, which are usually not relevant for classic free-standing blocks, becomes important when studying post-tensioned rocking systems. The results obtained suggest that the use of post-tensioned tendons becomes less advantageous when pulses of higher acceleration amplitude are considered, as the initial post-tensioning force can significantly amplify rotation and acceleration demands for initial force ratios that are common in practical applications ($P_0/W \leq 6$).

Finally, we assessed the alternative of using supplemental rotational inertia for the seismic control of post-tensioned rocking buildings. The proposed strategy employs inerters, a mechanical device that develops a resisting force proportional to the relative acceleration between its terminals. Our derivation of the equation of motion of the system shows that the inclusion of the inerter effectively reduces the frequency parameter of the wall resulting in lower seismic demands due to the well-known size effect of rocking behaviour. This result is then reasserted by the rocking spectra obtained for structures with typical post-uplift stiffness and initial post-tensioning force values subjected to Ricker acceleration pulses. Our analyses show that the introduction of the inerter further lowers the rotation response, while at the same time it significantly reduces the building accelerations levels. Nevertheless, this response enhancement does not translate into a significant reduction of the lateral forces, as the positive stiffness of the rocking walls is relatively low and the base shear is mainly controlled by the uplift resistance. Lastly, we conducted a probabilistic assessment of the seismic performance of protected and unprotected structures using a set of 202 real pulse-like acceleration records. The results of this assessment confirmed the behavioural trends observed under single pulse excitations, allowing us to conclude that the use of supplemental rotational inertia devices configures a practical alternative for modifying the dynamic response and reducing seismic demands in post-tensioned rocking building structures. However, further research is undergoing to analyse the efficiency of the system in taller structures, where the flexibility of the wall panels may not be neglected.

Acknowledgments

The authors gratefully acknowledge the financial support of CONICYT (Consejo Nacional de Ciencia y Tecnología, Chile); Grant No72170284.

References

References

[1] GW Housner. The Behavior of Inverted Pendulum Structures During Earthquakes. *Bulletin of the Seismological Society of America*, 53:403–417, 1963.

[2] M.J.N. Priestley. An overview of PRESSS research program. *PCI Journal*, 36(4), 1991.

[3] C. Christopoulos, A. Filiatrault, C. M. Uang, and B. Folz. Post-tensioned Energy Dissipating Connections for Moment Resisting Steel Frames. *ASCE Journal of Structural Engineering*, 128 9:1111–1120, 2002.

[4] LT Kibriya, C Málaga-Chuquitaype, and MM Kashani. Buckling-enabled composite bracing for damage-avoidance rocking structures. *International Journal of Mechanical Sciences*, 170:105359, 2020.

[5] Yahya Kurama. Hybrid post-tensioned precast concrete walls for use in seismic regions. *PCI Journal*, 47:36–59, 09 2002.

[6] Tony Holden, Jose Restrepo, and John B. Mander. Seismic performance of precast reinforced and prestressed concrete walls. *Journal of Structural Engineering*, 129(3):286–296, 2003.

[7] M.J.N. Priestley, S. Sritharan, J. R. Conley, and S. Pampanin. Preliminary Results and Conclusions from the PRESSS Five-story Precast Concrete Test-building. *PCI Journal*, 44(6):42–67, 1999.

[8] Stefano Pampanin, M. J. Nigel Priestley, and S. Sritharan. Analytical modelling of the seismic behaviour of precast concrete frames designed with ductile connections. *Journal of Earthquake Engineering*, 5(3):329–367, 2001.

[9] H A. Spieth, Athol Carr, A G. Murahidy, D Arnolds, M Davies, and J.B. Mander. Modelling of post-tensioned pre-cast reinforced concrete frame structures with rocking column connections. 01 2004.

[10] D. Pennucci, G. M. Calvi, and T. J. Sullivan. Displacement-based design of precast walls with additional dampers. *Journal of Earthquake Engineering*, 13(sup1):40–65, 2009.

[11] A. Iqbal, S. Pampanin, A. Palermo, and A. H. Buchanan. Performance and design of lvl walls coupled with ufp dissipaters. *Journal of Earthquake Engineering*, 19(3):383–409, 2015.

[12] Andre Filiatrault and Timothy Sullivan. Performance-based seismic design of nonstructural building components: The next frontier of earthquake engineering. *Earthquake Engineering and Engineering Vibration*, 13(1):17–46, Aug 2014.

[13] MF Vassiliou and N Makris. Dynamics of the Vertically Restrained Rocking Column. *J. Eng. Mech*, 141(12):04015049, 2015.

[14] L. F. Aragaw and P. M. Calvi. Earthquake-induced floor accelerations in base-rocking wall buildings. *Journal of Earthquake Engineering*, pages 1–29, 2018.

[15] I Calio and M Marletta. Passive control of the seismic rocking response of art objects. *Eng. Struct*, 25(8):1009–1018, 2003.

[16] R Ceravolo, ML Pecorelli, and L Zanotti Fragonara. Semi-active control of the rocking motion of monolithic art objects. *J. Sound Vib*, 374:1–16, 2016.

[17] MF Vassiliou and N Makris. Analysis of the rocking response of rigid blocks standing free on a seismically isolated base. *Earthq Eng Struct Dyn*, 41:177–196, 2012.

[18] N Makris and J Zhang. Rocking response of anchored blocks under pulse-type motions. *J. Eng. Mech*, 127:484–493, 2001.

[19] Rosario Ceravolo, ML Pecorelli, and Luca Zanotti Fragonara. Comparison of semi-active control strategies for rocking objects under pulse and harmonic excitations. *Mechanical Systems and Signal Processing*, 90:175–188, 2017.

[20] AM deLeo, G Simoneschi, C Fabrizio, and A DiEgidio. On the use of a pendulum as mass damper to control the rocking motion of a rigid block with fixed characteristics. *Meccanica*, 51(11):2727–2740, Nov 2016.

[21] MC Smith. Synthesis of mechanical networks: The Inerter. *IEEE Trans. Autom. Control*, 47(10):1648–1662, 2002.

[22] IF Lazar, SA Neild, and DJ Wagg. Using an inerter-based device for structural vibration suppression. *Earthq Eng Struct Dyn*, 43(8):1129–1147, 2014.

[23] Alin Radu, Irina F. Lazar, and Simon A. Neild. Performance-based seismic design of tuned inerter dampers. *Structural Control and Health Monitoring*, 26(5):e2346, 2019.

[24] Z Zhao, R Zhang, Y Jiang, and C Pan. A tuned liquid inerter system for vibration control. *International Journal of Mechanical Sciences*, 164:105171, 2019.

[25] Xiaoling Jin, Michael ZQ Chen, and Zhilong Huang. Minimization of the beam response using inerter-based passive vibration control configurations. *International Journal of Mechanical Sciences*, 119:80–87, 2016.

[26] D De Domenico, P Deastra, G Ricciardi, ND Sims, and DJ Wagg. Novel fluid inerter based tuned mass dampers for optimised structural control of base-isolated buildings. *Journal of the Franklin Institute*, 356(14):7626–7649, 2019.

[27] X Pan and C Málaga-Chuquitaype. Seismic control of rocking structures via external resonators. *Earthquake Engineering & Structural Dynamics*, 27(5):e2523, 2020.

[28] T Arakaki, H Kuroda, F Arima, Y Inoue, and K Baba. Development of seismic devices applied to ball screw. Part 1: Basic performance of test RD-series. *AIJ J.Technol. Des*, 8:239–244, 1999.

[29] N Makris and G Kampas. Seismic Protection of Structures with Supplemental Rotational Inertia. *Journal of Engineering Mechanics*, 142(11):1–11, 2016.

[30] C Málaga-Chuquitaype, C Menendez-Vicente, and R Thiers-Moggia. Experimental and numerical assessment of the seismic response of steel structures with clutched inerters. *Soil Dynamics and Earthquake Engineering*, 121:200–211, 03 2019.

[31] RW Clough and J Penzien. *Dynamics of structures*. McGraw-Hill, New York, 1975.

[32] A Chopra. *Dynamics of structures: Theory and applications to earthquake engineering*. International Series in Civil Engineering and Engineering Mechanics, Prentice Hall, Upper Saddle River, NJ, 2000.

[33] N Makris and G Kampas. Size versus slenderness: Two competing parameters in the seismic stability of free-standing rocking columns. *Bull. Seism. Soc. Am*, 106(1):104–122, 2016.

[34] R Thiers-Moggia and C Malaga-Chuquitaype. Seismic protection of rocking structures with inerters. *Earthquake Engng Struct Dyn*, 48:528–547, 2019.

[35] D Moroder, S Pampanin, A Palermo, T Smith, F Sarti, and A Buchanan. Diaphragm Connections in Structures with Rocking Timber Walls. *Structural Engineering International*, 27(2):165–174, 2017.

[36] Sinan Acikgoz and Matthew J DeJong. Analytical modelling of multi-mass flexible rocking structures. *Earthquake engineering & structural dynamics*, 45(13):2103–2122, 2016.

[37] R Thiers-Moggia. *Seismic protection of rocking structures with inerters, PhD Thesis*. Department of Civil and Environmental Engineering, Imperial College London, UK, 2020.

[38] EG Dimitrakopoulos and MJ DeJong. Revisiting the rocking block: closed-form solutions and similarity laws. *Proceedings of the Royal Society A: Mathematical, Physical and Engineering Sciences*, 468:2294–2318, 2012.

[39] N Ricker. Further developments in the wavelet theory of seismogram structure. *Bull. Seism. Soc. Am.*, 33(3):197–228, 1943.

[40] N Ricker. Wavelet functions and their polynomials. *Geophysics*, 9(3):314–323, 1944.

[41] MF Vassiliou and N Makris. Estimating time scales and length scales in pulselike earthquake acceleration records with wavelet analysis. *Bull. Seismol. Soc. Am.*, 101(2):596–618, 2011.

[42] K Ikago, K Saito, and N Inoue. Seismic control of single-degree-of-freedom structure using tuned viscous damper. *Earthquake Engineering and Structural Dynamics*, 41(3):436–474, 2012.

[43] C Málaga-Chuquitaype and K Bougatsas. Vector-im-based assessment of alternative framing systems under bi-directional ground-motion. *Engineering Structures*, 132:188–204, 2017.

[44] EG Dimitrakopoulos and TS Paraskeva. Dimensionless fragility curves for rocking response to near-fault excitations. *Earthquake engineering & structural dynamics*, 44(12):2015–2033, 2015.

[45] EG Dimitrakopoulos and AI Giouvanidis. Rocking amplification and strong-motion duration. *Earthquake Engng Struct Dyn*, pages 1–22, 2018.

[46] F. Jalayer and C. A. Cornell. Alternative non-linear demand estimation methods for probability-based seismic assessments. *Earthquake Engineering & Structural Dynamics*, 38(8):951–972, 2009.

[47] Eduardo Miranda and Shahram Taghavi. *A Comprehensive Study of Floor Acceleration Demands in Multi-Story Buildings*, pages 616–626. 2009.

[48] Comite Europeen de Normalization. *Eurocode 8 - Design Provisions for Earthquake Resistant Structures, EN-1998-1:2004: E.*

[49] Andrea Miano, Fatemeh Jalayer, Hossein Ebrahimian, and Andrea Prota. Cloud to ida: Efficient fragility assessment with limited scaling. *Earthquake Engineering & Structural Dynamics*, 47(5):1124–1147, 2018.

[50] Timothy Sullivan, Paolo M Calvi, and Roberto Nascimbene. Towards improved floor spectra estimates for seismic design. *Earthquakes and Structures*, 4(1):109–132, 2013.